proceedings

MDPI

Proceedings

Numerical Study of a Multi-Layered Strain Sensor for Structural Health Monitoring of Asphalt Pavement †

Jiayue Shen [1,*], Minghao Geng [1], Abby Schultz [1], Weiru Chen [2], Hao Qiu [3] and Xianping Wang [4]

[1] College of Engineering, SUNY Polytechnic Institute, Utica, NY 13502, USA
[2] Department of Information Technology and Decision Sciences, Old Dominion University, Norfolk, VA 23529, USA
[3] Department of Engineering Technology, Fort Valley State University, Fort Valley, GA 31030, USA
[4] Department of Computer Information Technology and Graphics, Purdue University Northwest, Hammond, IN 46323, USA
* Correspondence: shenj@sunypoly.edu
† Presented at the 6th International Electronic Conference on Sensors and Applications, 15–30 November 2019; Available online: https://ecsa-6.sciforum.net/.

Published: 14 November 2019

Abstract: Crack initiation and propagation vary the mechanical properties of the asphalt pavement and further alter its designate function. As such, this paper describes a numerical study of a multi-layered strain sensor for the structural health monitoring (SHM) of asphalt pavement. The core of the sensor is an H-shaped Araldite GY-6010 epoxy-based structure with a set of polyvinylidene difluoride (PVDF) piezoelectric transducers in its center beam, which serve as a sensing unit, and a polyurethane foam layer at its external surface which serves as a thermal insulation layer. Sensors are coated with a thin layer of urethane casting resin to prevent the sensor from being corroded by moisture. As a proof-of-concept study, a numerical model is created in COMSOL Multiphysics to simulate the sensor-pavement interaction, in order to design the strain sensor for SHM of asphalt pavement. The results reveal that the optimum thickness of the middle polyurethane foam is 11 mm, with a ratio of the center beam/wing length of 3.2. The simulated results not only validate the feasibility of using the strain sensor for SHM (traffic load monitoring and damage detection), but also to optimize design geometry to increase the sensor sensitivity.

Keywords: strain sensor; asphalt pavement; crack detection

1. Introduction

Crack initiation and propagation vary the mechanical properties of the pavement and further alter its designed function [1]. To date, optical fibers [2], conventional strain gauges [3], and sometimes metal-foil-type gauges [4], are commonly used for Structural Health Monitoring (SHM) applications. Although conventional strain gauges show good reliability, they are rarely used in asphalt materials, due to the challenges of harsh installation conditions, high temperatures (up to 164 °C), and pressure (around 290 ksi) [5,6]. Optical fibers are relatively expensive.

Piezoelectric materials are materials that can generate electrical charges when they are mechanically deformed. To date, piezoelectric materials, such as piezoceramic material (Lead Ziroconate Titanate, PZT) and piezoelectric plastic material (PVDF), have been widely used in research and in practice as sensors for dynamic applications in SHM and energy harvest [7–10], since piezoelectric-based sensors have strong piezoelectric effects and wide bandwidth. However, piezoceramic material always suffers from saturation due to its high piezoelectric coefficient, and is also far too brittle to sustain

high strain. Piezoelectric plastic materials, such as PVDF, offer the advantages of high sensitivity, good flexibility, good manufacturability, small distortion, low thermal conductivity, high chemical corrosion resistance, and heat resistance [11,12]. As such, PVDF was chosen as the key sensing material for this multi-layered strain sensor. However, due to the harsh installation conditions of the asphalt pavement, particularly the high temperature (up to 164 °C) and pressure (around 290 ksi), specific packaging would need to be designed for the PVDF thin film to survive during the construction.

To this end, this work proposes to use a multi-layered strain sensor to overcome the installation challenges in asphalt pavement and to provide a reliable SHM approach of asphalt pavement. The core of the sensor is an H-shaped Araldite GY-6010 epoxy structure with a set of PVDF piezoelectric transducers in its center beam and a polyurethane foam layer at its external surface. A thin layer of a cast urethane resin coating and Araldite GY-6010 epoxy frameset are added to enhance the overall sensor stiffness and to prevent the sensor's being damaged in the field by compaction. The H-shape is adopted from the conventional strain gauge [13]. As a proof-of-concept study, a numerical stress deflection model was created to simulate the pavement-sensor interaction for the design of the strain sensor for monitoring the SHM of asphalt pavement. Simulation of heat transfer is conducted in COMSOL to determine the thickness of each layer. As a result, the chosen thickness of the middle foam layer is 11 mm. Another finite element analysis was conducted to study the center beam length/wing length ratio and to validate the sensor's capability of capturing the crack initiation after packaging.

2. Sensor Configuration

Figure 1 depicts the multi-layered strains sensor used in this work for the SHM of asphalt pavement. The key sensing unit is an 80 mm × 18 mm × 1.55 mm PVDF piezoelectric thin film [13]. To better protect the PVDF thin film, three layers of protection, which respectively are the internal mechanical protection layer, the middle thermal insulation layer, and the outmost corrosion protection layer made by urethane casting resin, are built on the external surface of the PVDF thin film. Regarding the internal mechanical protection layer, the packaging material chosen is Araldite GY-6010 epoxy [5]. According to the material parameter sheet of Araldite GY-6010 epoxy, it has a tensile modulus around 2.67 GPa and high tensile and flexural strengths above 27.56 MPa, which are similar to other epoxies. Its thermal conductivity is relatively lower, generally only 0.2 $W \cdot m^{-1} \cdot K^{-1}$. In addition, polyurethane foam is chosen as the material for the middle thermal insulation layer due to its excellent thermal insulation performance. The thermal conductivity of polyurethane foam is only 0.022 $W \cdot m^{-1} \cdot K^{-1}$ [14]. Considering the stress distribution of the sensor embedded underneath the pavement, the H-shape has been adopted in this paper. The thickness of the outer corrosion protection layer is less than 1 mm, which is negligible as compared with the thickness of the other two layers, and it will not be discussed in this paper. The substitute was not included in the analysis.

As mentioned above, the thermal insulation material used in this study is polyurethane foam, which has a thermal conductivity of 0.022 $W \cdot m^{-1} \cdot K^{-1}$ [14]. Several heat conduction simulations are conducted to determine the thickness of the foam. To simply the finite element model (FEM), a two-dimensional FEM is created in COMSOL Multiphysics, as shown in Figure 2b according to the conduction Equations (1) and (2).

$$d_z \rho C_p \frac{\partial T}{\partial t} + d_z \rho C_p u \cdot \nabla T + \nabla \cdot q = d_z Q + q_0 + d_z Q_{ted}, \quad (1)$$

$$q = -d_z k \nabla T, \quad (2)$$

where Q is the heat content in Joules, k represents the conductivity of materials which used in the simulation, q is the local heat flux density, $W \cdot m^{-2}$, and ρ is the density of each material, $kg \cdot m^{-3}$. C_p is each material's specific heat capacity, $J \cdot kg^{-1} \cdot K^{-1}$. ∇T is the temperature gradient, $K \cdot m^{-1} \cdot T$, t represents the temperature and the time, respectively.

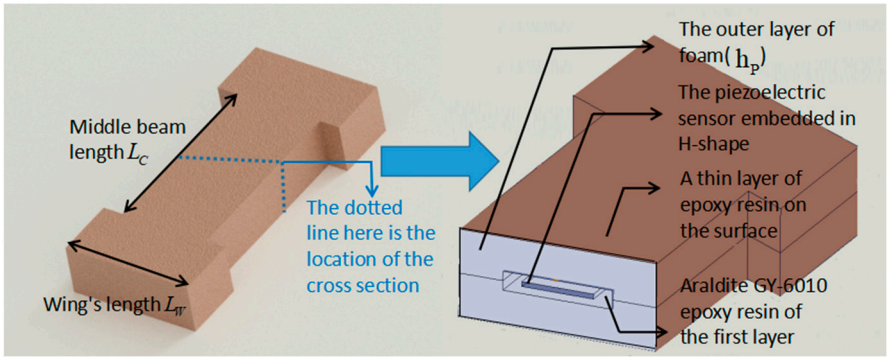

Figure 1. Configuration of the multi-layered strain sensor.

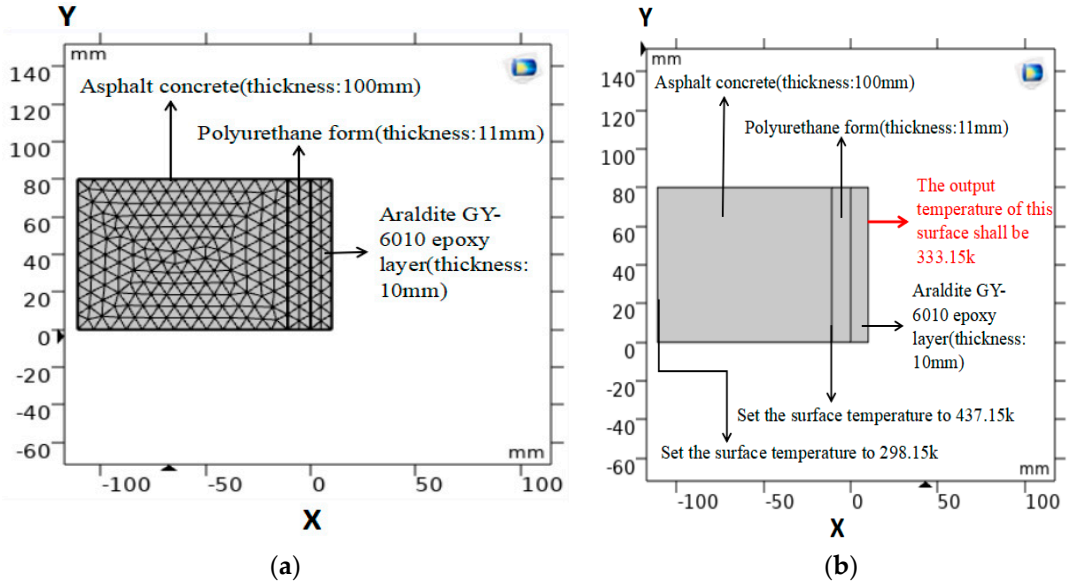

Figure 2. (**a**) 2D finite element model (FEM) with 422 elements; (**b**) schematic of 2D model with boundary conditions. Note the temperature in red is the output temperature captured after the heat transfer analysis and it is not one of the boundary conditions.

In the FEM, the thickness of the polyurethane foam is simulated in the range of 5 mm to 12 mm with a 1 mm increment. Meanwhile, the thicknesses of the asphalt concrete and the internal mechanical protection layer (Araldite GY-6010 epoxy layer) are set as 100 mm and 10 mm, respectively. The thickness of the internal mechanical protection layer is an estimate value based on the desired mechanical strength of the sensor. The boundary condition of the model is set as shown in Figure 2a. The left boundary of the asphalt is directly in contact with air, whose temperature is set as constant room temperature: 298.15 K. Meanwhile, the right boundary of the asphalt is in contact with the strain sensor, whose temperature should initiate at 437.15 K [15]. Finally, according to the literature, the average cooling time of the asphalt pavement is 39 mins [15]. As such, the heat transfer time in this study is set as 39 mins. As a result, the maximum output temperature (the temperature between the middle mechanical protection layer and PVDF thin film) should be no more than 333.15 K (the item labeled in red in Figure 2a). In Figure 2a,b and Figure 3, the X axis and Y axis represent the directions along the sensor height and length, respectively.

As shown in Figure 3, with the increase of the foam thickness, the output temperature drops correspondingly. If the desired output temperature is 333.15 K (60 °C), the minimum thickness of the foam should be 11 mm. It can be clearly seen from Figure 4 that the output temperature decreases dramatically after the thermal insulation layer (foam layer).

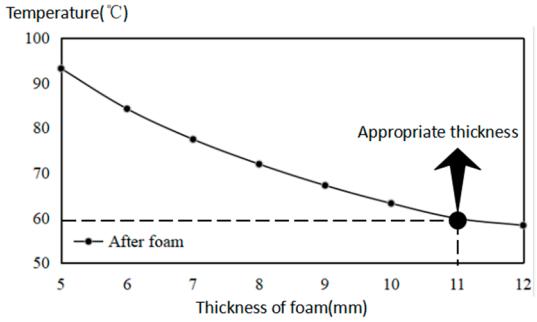

Figure 3. The relation between the foam thickness and output temperature.

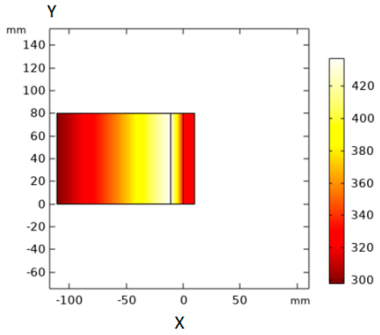

Figure 4. Finite element simulation of the temperature distributions when the thickness of asphalt, polyurethane foam and epoxy are 100 mm, 11 mm, and 10 mm.

3. Solid Mechanics Model

3.1. Finite Element Model

After the determination of the thickness of the middle thermal insulation layer, the next important task is to determine the optimal ratio of the wing length to the center beam length. With the optimal ratio, the sensor is expected to reach its highest sensitivity with the lowest material cost, in other words, the lowest cost. Considering the pressure on the road, the static performance of the sensor under the pressure of the car (4900 N) on the road is simulated and analyzed. In this simulation, the length of the center beam of the H-shape, L_C, is first fixed as 160 mm, and the strain is observed by varying the wing length, L_W, in the range of 20 mm to 50 mm with a 10 mm increment. After confirming the length of the wing, L_W, another simulation is carried out to determine the final center beam length/wing length ratio by fixing the wing length at 50 mm and varying the center beam length in the range of 80 mm to 200 mm with a 20 mm increment.

3.2. Three-Point Bending Test

In this simulation, a three-point bending test is utilized to analyze the sensor design. As shown in Figure 5, two concrete supports are used at both ends of the bottom of asphalt pavement beam. The size of the asphalt concrete is 300 mm × 130 mm × 100 mm. The thickness of the asphalt equals 100 mm, cited from Alavi, A.H.'s study [16]. A force of 4.9 kN is applied to the middle region of the asphalt pavement beam's top surface, with a contact area of 200 mm × 130 mm. In other words, the overall pressure applied on the top of the beam is about the pressure of a tire on the ground of an ordinary car.

In addition, the same analysis is also used to validate the feasibility of using the sensor to detect the pavement crack. The damage was introduced by making a crack at the middle of the bottom of the asphalt pavement beam. To be consistent, the total height of the asphalt pavement beam is still 100 mm (D = 100 mm). By increasing the crack depth, D_C, the measured sensor strain should change correspondingly. As such, the crack depth, D_C, is chosen in the range of 0 mm to 100 mm with a 10

mm increment. In the FEM, the Elastic modulus, the density, and Poisson's ratio of asphalt pavement beam used were 1200 MPa, 2.6 g·cm^{-3}, and 0.35, respectively.

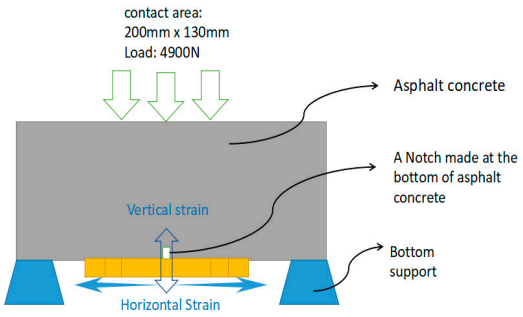

Figure 5. Schematic of the Three-point Bending Test Setup in the simulation.

3.3. Result and Discussion

Figure 6 shows that with the increase of the wing length, L_W, both the vertical and the horizontal strain increases. However, when the wing length, L_W, increases to 50 mm, the vertical strain curve begins to flatten and it stabilizes at around 101 με. Meanwhile, the horizontal strain first shows a gentle trend and then shows a sharp upward trend. Therefore, according to the variation trend of the water vertical strain curve, 50 mm can be determined as the suitable width of the wing. After determining the width of the wing, the simulation began to change the length of the center beam, L_C, with a fixed side wing length, L_W. The simulation results are shown in Figure 7; by increasing the length of the center beam, the two strain curves increase gradually until the length of the center beam, L_C, reaches 160 mm. After 160 mm, the horizontal strain basically does not change, but the vertical strain curve drops slightly in the range of 160 mm to 180 mm. Then both the vertical strain and the horizontal strain show a peak at 190 mm. When the length reaches 200 mm, the two curves decrease sharply, indicating that the performance of the H-shape cannot be guaranteed. As such, the final decision is to use 160 mm as the length of the final center beam. In other words, the optimal ratio of the center beam length (160 mm) to wing length (50 mm) is Section 3.2.

The simulation results of crack detection are shown in Figure 8. It can be clearly seen from the figure that when the notch depth increases to 50 mm, the two strain curves reach their peaks. From 50–90 mm, these two curves drop slightly. After 90 mm, the strain value begins to decline. Therefore, it can be concluded that the H-shape can detect the state of the crack by observing the vertical strain or the horizontal strain.

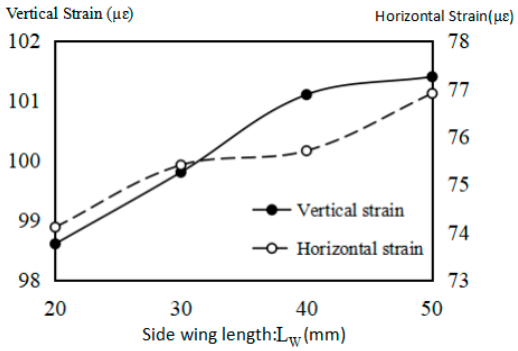

Figure 6. Strain changes: wing length = 20 mm~50 mm, center beam length = 160 mm.

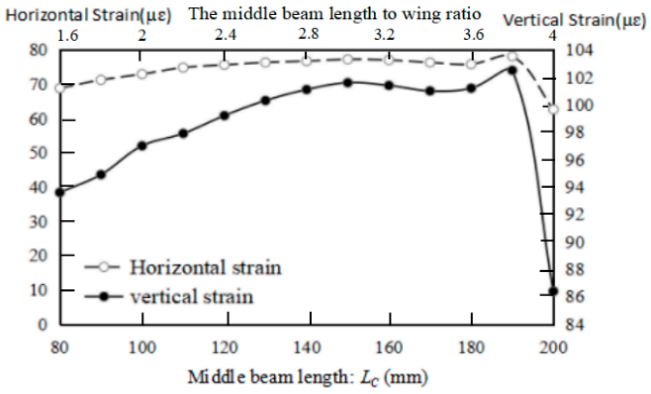

Figure 7. Strain changes: wing length = 50 mm, center beam length = 80 mm~200 mm.

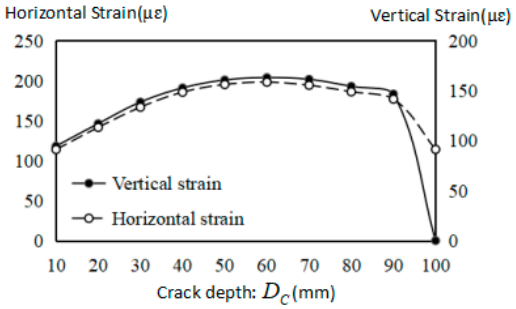

Figure 8. The strain of H-shape changes with the increase of notch.

4. Conclusions

In this paper, a unique sensor package is designed to detect cracks in the bottom of asphalt concrete on the road. The selection of packaging materials, the thickness of packaging materials, and the shape of packaging were all simulated to determine the dimensions of packaging. Although the package design of the piezo-sensor has been simulated by many groups, and its feasibility has been proved by the results, there are still many problems to be solved when considering various road and environmental loads. The main problems are as follows: The manufacturing process of the H-shape is complex and time-consuming; the physical and chemical properties of the H-shape surface need further verification as to whether it is suitable for its working environment; only a few types of structures can be analyzed; and the H-shape may not be the best packaging shape. Future research is needed to find better shapes to replace the H-shape. Numerical simulations will help in choosing the ideal stress condition, since valid data can be difficult to collect in the actual use situation.

Author Contributions: Conceptualization, J.S. and W.C.; methodology, J.S. and M.G.; software, W.C., M.G.; validation, M.G. and A.S.; data analysis, J.S. and M.G.; investigation, J.S. and M.G.; resources, J.S., M.G. and W.C.; data curation, J.S. and M.G.; writing—original draft preparation, J.S. and M.G.; writing—review and editing, W.C., H.Q. and X.W.; visualization, J.S. and M.G.; supervision, J.S.; project administration, J.S. All authors have read and agree to the published version of the manuscript. All authors have read and agreed to the published version of the manuscript.

Funding: This research received no external funding.

Conflicts of Interest: The authors declare no conflict of interest.

References

1. Castell, M.A.; Ingraffea, A.R.; Irwin, L.H. Fatigue crack growth in pavements. *J. Traffic Transp.* **2000**, *126*, 283–290.
2. Li, H.N.; Li, D.S.; Song, G.B. Recent applications of fiber optic sensors to health monitoring in civil engineering. *Eng. Struct.* **2004**, *26*, 1647–1657.

3. Takeda, S.; Aoki, Y.; Ishikawa, T.; Takeda, N.; Kikukawa, H. Structural health monitoring of composite wing structure during durability test. *Compos. Struct.* **2007**, *79*, 133–139.
4. Jo, H.; Park, J.W.; Spencer, B.F.; Jung, H.J. Development of high-sensitivity wireless strain sensor for structural health monitoring. *Smart Struct. Syst.* **2013**, *11*, 477–496.
5. Lajnef, N.; Chatti, K.; Chakrabartty, S.; Rhimi, M.; Sarkar, P. *Smart Pavement Monitoring System (No. FHWA-HRT-12-072)*; *Federal Highway Administration*, East Lansing, MI, USA, 2013.
6. Kim, Y.R.; Seo, Y.; King, M.; Momen, M. Dynamic modulus testing of asphalt concrete in indirect tension mode. *Transp. Res. Rec.* **2004**, *1891*, 163–173.
7. Kaur, N.; Li, L.; Bhalla, S.; Xia, Y.; Ni, P.; Adhikari, S. Integration and evaluation of multiple piezo configurations for optimal health monitoring of reinforced concrete structures. *J. Intell. Mater. Syst. Struct.* **2017**, *28*, 2717–2736.
8. Kaur, N.; Bhalla, S. Combined energy harvesting and structural health monitoring potential of embedded piezo-concrete vibration sensors. *J. Energy Eng.* **2014**, *141*, D4014001.
9. Audrain, P.; Masson, P.; Berry, A.; Pascal, J.C.; Gazengel, B. The use of PVDF strain sensing in active control of structural intensity in beams. *J. Intell. Mater. Syst. Struct.* **2004**, *15*, 319–327.
10. Cahill, P.; Hazra, B.; Karoumi, R.; Mathewson, A.; Pakrashi, V. Vibration energy harvesting based monitoring of an operational bridge undergoing forced vibration and train passage. *Mech. Syst. Signal Process.* **2018**, *106*, 265–283.
11. Ambrosy, A.; Holdik, K. Piezoelectric PVDF films as ultrasonic transducers. *J. Phys. E Sci. Instrum.* **1984**, *17*, 856.
12. Wang, H.; Liu, Z.; Wang, E.; Zhang, X.; Yuan, R.; Wu, S.; Zhu, Y. Facile preparation of superamphiphobic epoxy resin/modified poly (vinylidene fluoride)/fluorinated ethylene propylene composite coating with corrosion/wear-resistance. *Appl. Surf. Sci.* **2015**, *357*, 229–235.
13. Xiao, J.; Zou, X.; Xu, W. ePave: A self-powered wireless sensor for smart and autonomous pavement. *Sensors* **2017**, *17*, 2207.
14. Wu, J.W.; Sung, W.F.; Chu, H.S. Thermal conductivity of polyurethane foams. *Int. J. Heat Mass Transf.* **1999**, *42*, 2211–2217.
15. García, A.; Norambuena-Contreras, J.; Partl, M.N. Experimental evaluation of dense asphalt concrete properties for induction heating purposes. *Constr. Build. Mater.* **2013**, *46*, 48–54.
16. Alavi, A.H.; Hasni, H.; Lajnef, N.; Chatti, K.; Faridazar, F. An intelligent structural damage detection approach based on self-powered wireless sensor data. *Automat. Constr.* **2016**, *62*, 24–44.